Available online at www.sciencedirect.com
ScienceDirect
Journal of Sound and Vibration 298 (2006) 84–107
JOURNAL OF SOUND AND VIBRATION
www.elsevier.com/locate/jsvi

Optimization of damping and absorbing performance of shunted piezo elements utilizing negative capacitance

Marcus Neubauer[a,*], Robert Oleskiewicz[b], Karl Popp[a,†], Tomasz Krzyzynski[b]

[a]*Institute of Dynamics and Vibrations, University of Hannover Appelstr. 11, D-30167 Hannover, Germany*
[b]*Department of Mechatronics, Faculty of Mechanical Engineering, Koszalin University of Technology, Raclawicka 15-17, PL 75-620 Koszalin, Poland*

Received 27 June 2005; received in revised form 21 April 2006; accepted 24 April 2006
Available online 13 July 2006

"The authors dedicate this article to the memory of their colleague, Professor Karl Popp who initiated the research"

Abstract

In this paper, the effect of negative capacitance in damping and absorbing systems using shunted piezoelectric transducers is analyzed. Different passive and semi-active configurations of networks have been compared in a general, normalized form, highlighting the influence of the general electromechanical coupling coefficient and the negative capacitance. Commonly used criteria for passive networks are adapted to the general configuration with negative capacitance resulting in optimal parameters. The damping and absorbing performance of optimal passive and semi-active networks are compared. With optimal parameter for negative capacitance, an upper limit for maximum appearing amplitude in the frequency response function (FRF) can be given. Results are verified experimentally using a test rig.

1. Introduction

Piezo elements have the unique ability to transfer mechanical energy into electrical energy and vice versa. By connecting suitable networks containing resistive and inductive elements to the electrodes of the piezo element, an electromechanical vibration damper or vibration absorber can be created. These networks can be tuned to minimize the maximum amplitude of the frequency response function and thus resulting in broadband damping [1]. In analogy to mechanical absorbing systems, the absorbing effect deteriorates with increased damping, so the optimal performance can be achieved using an inductance only. Because of the narrow bandwidth of the absorbed frequencies the resulting system is very sensitive to tuning errors and variations of the excitation frequency.

To overcome these problems, Corr and Clark [2] analyzed switching shunt techniques for structural damping. They suggest a state switching and a pulse switching within one vibration cycle. In state switching,

*Corresponding author. Tel.: +49 511 762 4168.
E-mail addresses: neubauer@ifm.uni-hannover.de (M. Neubauer), r.oleskiewicz@wp.pl (R. Oleskiewicz), tkrzyz@tu.koszalin.pl (T. Krzyzynski).
†Deceased.

0022-460X/$ - see front matter © 2006 Elsevier Ltd. All rights reserved.
doi:10.1016/j.jsv.2006.04.043

Nomenclature

A_p	surface area of electrodes
c_0	mechanical spring
c_{33}	stiffness of the piezo element
c_{sd}	stiffness of mechanical spring in the equivalent mechanical model
C	external capacitance
C_{ps}	capacitance of the piezo element
d_0	mechanical damping element
d_{33}	charge density per unity stress under constant electric field
d_{sd}	damping element of the equivalent mechanical model
D	generalized external resistance
D_0	generalized damping
D_E	electrical displacement
e	piezoelectric constant
E	electrical field
i_p	current flowing through the circuit
K_{3i}	generalized electromechanical coupling coefficient
K_E	modulus of elasticity
l_p	height of piezoceramics
L	external inductance
m	main mass
R	external resistance
s	mechanical strain
u_p	voltage on the electrodes
γ	square of the generalized electromechanical coupling coefficient
δ	inverse of the generalized external capacitance
ε_S	electrical permittivity
η	normalized frequency
λ	generalized external inductance
ω_m	eigenfrequency of the mechanical system
Ω	angular velocity of external force

damping is achieved by removing strain energy from the mechanical system when switching between open- and short-circuit electrodes. This is caused by a change of stiffness of piezo element, thus it is only usable when the stiffness of the piezo element dominates the overall system stiffness. In pulse switching the piezo element is briefly connected to a inductor/resistor shunt circuit, which allows a generated charge to be applied to the piezo element similar to direct velocity feedback control. A comparison of these techniques showed nearly the same damping performance for the pulse-switching and traditional passive tuned resonance circuits. The advantages of the switching techniques are a smaller required shunt inductance, a lower sensitivity to environmental changes and easier tuning. Morgan and Wang [3] approached this problem by utilizing a combination of a passive electrical circuit and active control actions to synthesize a system for adaptive variable frequency narrowband disturbance rejection, where the active control consists of an inductor tuning action, a negative resistance action and a coupling enhancement action. Niederberger et al. [4] introduced a new technique for online adaptation of multi-mode resonant shunts. Circuit component values are tuned online by minimizing the relative phase difference between a vibration reference signal and the shunt branch current. They achieved a simultaneous damping of up to four structural modes.

Tang and Wang [5] compared different passive networks containing resistive and inductive networks and proved that they obtain nearly the same passive damping ability and driving source amplification characteristics. Further more, they proposed a method to increase the electro-mechanical coefficient by using a synthetic negative capacitance circuit, which was analyzed and experimentally verified. A negative capacitance circuit is capable of controlling the elasticity of the piezo element. Date et al. [6] achieved a change of the elastic constant of poled PVDF film samples between 0.5 and 2 times the original value. They present two networks representing a negative capacitance that are used to soften resp. harden the elastic coefficient. Also Fukada et al. [7] proved the efficiency of negative capacitance circuit connected to a curved PVDF film in sound isolation application. Changing the elasticity of the piezo film, the overall transmission loss level of 40 dB was achieved. The basic techniques for vibration absorbing using LR-networks can be generalized for multiple mode vibration suppression. Hollkamp [8] suggested a shunt circuit consisting of an LR-circuit for the first mode and additional parallel RLC (with a positive capacitance) shunts for each additional mode. However, previous resistive and inductive elements have to be retuned when a new shunt is added, and no closed-form tuning solution has been proposed yet. Behrens et al. [9] introduced the "current flowing" technique for piezoelectric shunt damping. The passive shunt controller consists of a specific number of resonant impedance branches depending on number of frequencies that are to be damped. Although the

presented solution has numerous technical advantages such like simpler structure in comparison with the one proposed by Wu [10], it is still very sensitive for piezo element capacitance variation, and does not solve the problem with the narrow bandwidth of absorbing area. Using the negative capacitance allows reducing the inductance requirements significantly in resonant circuits with no loss of the absorbing performance. It was shown already by Fleming et al. [11] that connecting the positive capacitance in parallel to a piezo patch can reduce the inductor value in resonant circuit. The inductance value is reduced by the same factor in which the capacitance of piezo element is increased, but the method is occupied with a lower controller gain and performance.

2. Semi-active shunt damping

Systems with passive networks containing resistive and inductive elements have numerously been examined and criteria and solutions for optimal parameters are given. Also, networks containing a negative capacitance have been discussed, indicating an increase of the coupling coefficient and therefore damping and absorbing performance. But there is still a lack of criteria for optimal tuning of such LRC-networks. Results for optimal parameter of the shunted network in a serial application will be given in this paper. Throughout all sections, the effect of the general coupling coefficient is highlighted. The results of the optimal R, LR and LRC-networks are compared with respect to the general coupling coefficient.

The proposed LRC-networks with a negative capacitance is a semi-active control. Compared to an active control, the semi-active approach offers a similar enhanced performance as active methods. By adjusting the dynamic properties of the host structure, the mechanical dissipation of the system can be largely increased. Therefore the semi-active control cannot cause instabilities, assuming that the original system was stable. The amount of power needed for the vibration control typically is significantly smaller than in an purely active control.

For an experimental verification of the results, a test rig has been established. In contrast to many experimental investigations using cantilevered beams, here a translational vibration system with a relatively high eigenfrequency of 1640 Hz is used. The analytical results of the damping and absorbing performances are validated by measurements.

The paper is arranged in the following order: The equations of the mechanical model under investigation connected with a LRC-network in serial application are established and normalized. Based on these equations any combination of the network is analyzed. Firstly, such networks are described, which contain only passive elements (L, R and LR-networks), and the optimal parameters for damping and absorbing are given. This is followed by a section describing the effect of a (negative) capacitance (C) only. In the following sections, the networks including a capacitance (LC, RC and LRC-networks) are discussed. The results are compared with the networks without a capacitance. Finally, a test rig and network representing the negative capacitance are introduced and measurements underlining the analytical results are shown.

3. Equations of motion

The system under investigation is depicted in Fig. 1. It consists of a mass m connected to a spring-damper (c_0, d_0) and a piezo element. The mass is excited by a harmonic force $F(t)$. The piezo element is represented as a spring c_{33} in the mechanical path and as a capacitance C_{ps} and a charge source in the electrical path. The mechanical and electrical systems are coupled by the following two equations:

$$\begin{aligned} \sigma &= K_E s - eE, \\ D_E &= es + \varepsilon_s E. \end{aligned} \tag{1}$$

Here, the following notation has been used: σ is the mechanical stress, K_E the modulus of elasticity, s the strain, e the piezoelectric constant, E the electrical field, D_E the electrical displacement, ε_s the electrical permittivity. Assuming that the force acting on the piezo element only affects changes in longitudinal direction, all elements in Eq. (1) are scalars. Force direction is the same as poling direction of the piezo element. In order to derive the equations connecting the force of the piezo element, the voltage on the

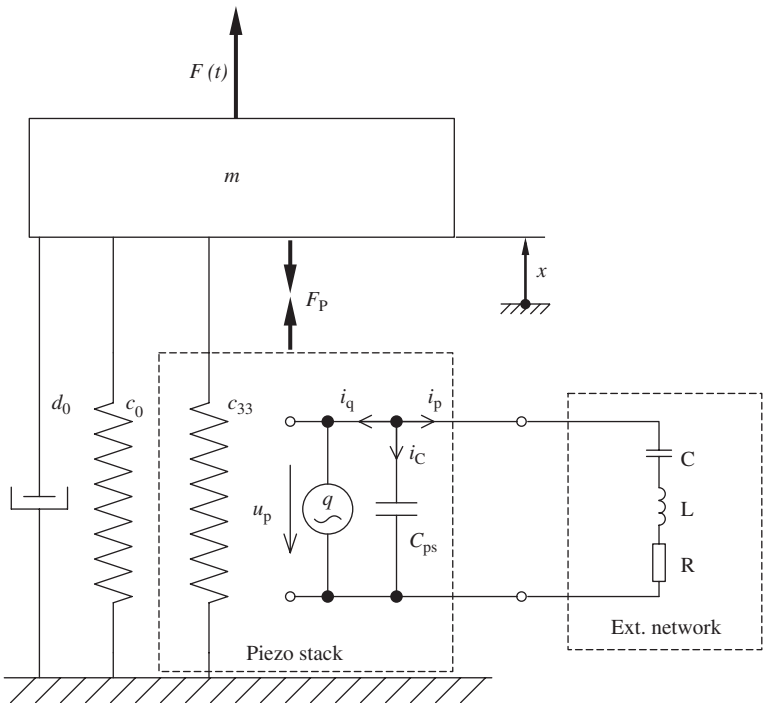

Fig. 1. Mechanical model with piezo element connected to external LRC-network.

electrodes, and the current flowing to the external network it is necessary to find the charge Q_p on the plates of the piezo ceramics. The electrical displacement D_E and the electric field E describing the capacitor that is formed by electrodes on top and bottom of the piezo material read, respectively,

$$D_E = \frac{Q_p}{A_p}, \quad E = \frac{u_p}{l_p}, \tag{2}$$

where A_p is the surface of electrodes, l_p the distance between electrodes (height) and u_p the voltage. The charge is found by substituting the strain in Eq. (1) with $s = x/l_p$,

$$Q_p = e\frac{A_p}{l_p}x + \varepsilon_S \frac{A_p}{l_p}u_p, \tag{3}$$

where x is the displacement of the top of the piezo stack. The term $\varepsilon_S A_p/l_p$ in Eq. (3) is the capacitance C_{ps} of the piezo element, where the electrical permittivity ε_S is the product of the vacuum and relative permittivities ε_0 and ε_r of the piezo ceramics. The piezoelectric constant can be described as

$$e = K_E d_{33}, \quad K_E \frac{A_p}{l_p} = c_{33}, \tag{4}$$

where d_{33} is the charge density per unity stress under a constant electric field and c_{33} the mechanical stiffness of the piezo material. The current i_p flowing to the external network is the first derivative of the charge with respect of time, resulting in

$$i_p + c_{33}d_{33}\dot{x} + C_{ps}\dot{u}_p = 0. \tag{5}$$

The mechanical stress σ of the piezo element in Eq. (1) is determined by the force acting on the surface,

$$\sigma = \frac{F_p}{A_p}. \tag{6}$$

By inserting Eq. (4) into Eq. (1) the force produced by the piezo element is found

$$F_p = c_{33}x - c_{33}d_{33}u_p. \tag{7}$$

So, it can be shown that the influence of the piezo element is totally described by parameters c_{33}, d_{33} and C_{ps}. The equation of the mechanical model reads

$$m\ddot{x} + d_0\dot{x} + c_0x + F_p = F(t), \tag{8}$$

excited by the external force $F(t)$. A harmonic force with angular velocity Ω is assumed,

$$F(t) = \hat{F}\,\sin(\Omega t). \tag{9}$$

The equation for the electrical network consisting of a RLC serial shunt branch reads

$$0 = u_p + L\frac{\mathrm{d}i_p}{\mathrm{d}t} + Ri_p + \frac{1}{C}\int i_p \mathrm{d}t \tag{10}$$

and determines the sum of voltages present on all network elements and the piezo element. It is described by the parameters L, R and C, where C can be positive or negative with a negative value indicating a negative capacitance. With the displacement x and the voltage u_p as degrees of freedom, the dynamical behavior of the system is given by

$$\begin{bmatrix} m & 0 \\ c_{33}d_{33}L & C_{ps}L \end{bmatrix}\begin{bmatrix} \ddot{x} \\ \ddot{u}_p \end{bmatrix} + \begin{bmatrix} d_0 & 0 \\ c_{33}d_{33}R & C_{ps}R \end{bmatrix}\begin{bmatrix} \dot{x} \\ \dot{u}_p \end{bmatrix} + \begin{bmatrix} c_0 + c_{33} & -c_{33}d_{33} \\ \frac{c_{33}d_{33}}{C} & 1 + \frac{C_{ps}}{C} \end{bmatrix}\begin{bmatrix} x \\ u_p \end{bmatrix} = \begin{bmatrix} F(t) \\ 0 \end{bmatrix}. \tag{11}$$

Ahlers [12] suggested a mechanical replacement model that has identical dynamical behavior as a piezo element connected with a LR-network in serial application. This model is now extended by a spring c_δ to cover the influence of the additional capacitance, cp. Fig. 2,

$$\begin{bmatrix} m & 0 \\ 0 & m_p \end{bmatrix}\begin{bmatrix} \ddot{x}_1 \\ \ddot{x}_2 \end{bmatrix} + \begin{bmatrix} d_0 & 0 \\ 0 & d_{sd} \end{bmatrix}\begin{bmatrix} \dot{x}_1 \\ \dot{x}_2 \end{bmatrix} + \begin{bmatrix} c_0 + c_{33} + c_{sd} & -c_{sd} \\ -c_{sd} & c_{sd} + c_\delta \end{bmatrix}\begin{bmatrix} x_1 \\ x_2 \end{bmatrix} = \begin{bmatrix} F(t) \\ 0 \end{bmatrix}. \tag{12}$$

The first degree of freedom is the displacement of the main mass, $x_1 = x$, and the second one reads $x_2 = x + u_pC_{ps}/c_{33}d_{33}$. This leads to diagonal mass and damping matrices.

In the absence of the spring c_δ, the mechanical replacement model is similar to a tuned mass damper. Consider that the damping element is placed between the oscillating mass and the reference frame, which corresponds to a skyhook damper arrangement.

In the following, normalized parameters are used introducing the non-dimensional time τ:

$$\begin{aligned} &\tau = \omega_m t, \quad \dot{x} = \omega_m x', \quad \omega_m^2 = \frac{c_0 + c_{33}}{m}, \quad \eta = \frac{\Omega}{\omega_m}, \\ &2D_0 = \frac{d_0}{\sqrt{(c_0 + c_{33})m}}, \quad 2D = RC_{ps}\omega_m, \quad \lambda = LC_{ps}\omega_m^2, \quad \delta = \frac{C_{ps}}{C}. \end{aligned} \tag{13}$$

The properties of the piezo element beside of the mechanical stiffness can all be condensed in a parameter γ,

$$\gamma = \frac{(c_{33}d_{33})^2}{C_{ps}(c_0 + c_{33})}, \tag{14}$$

that is the square of the generalized electromechanical coupling coefficient K_{3i},

$$K_{3i}^2 = \frac{\eta_n^{D^2} - \eta_n^{E^2}}{\eta_n^{E^2}}, \tag{15}$$

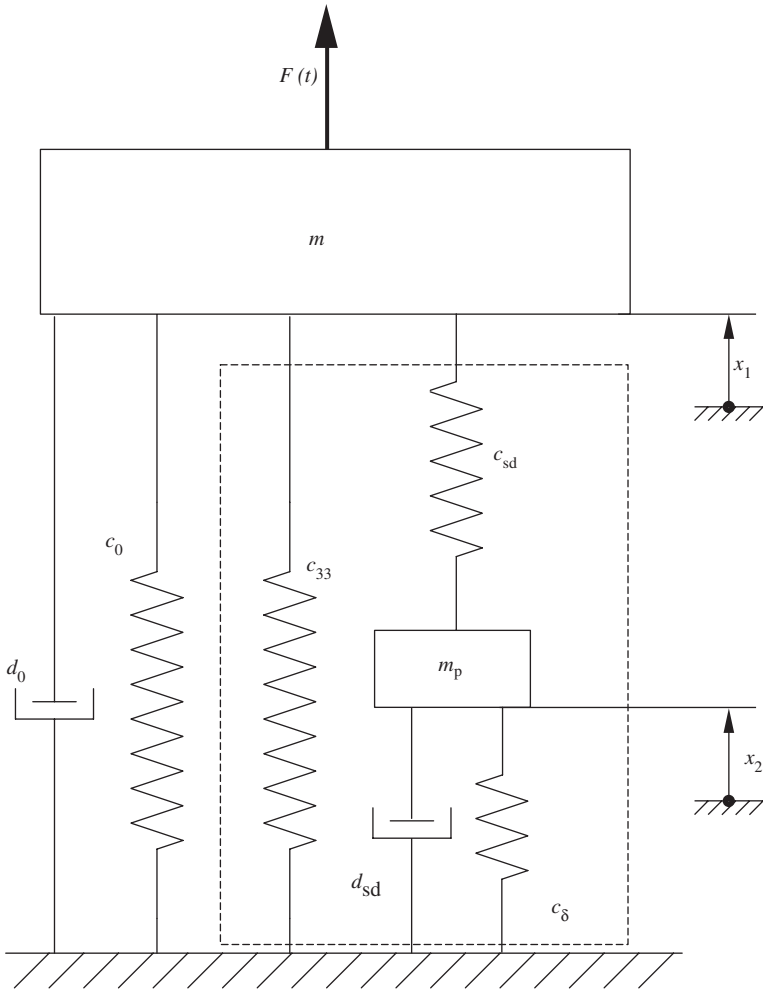

Fig. 2. Mechanical replacement model.

where $\eta_n^D = \sqrt{1+\gamma}$ and $\eta_n^E = 1$ are resonance frequencies for the open- and short-circuit electrodes, respectively (cf. R-network section). The equation of motion with normalized parameter read

$$\begin{bmatrix} 1 & 0 \\ 0 & \lambda \end{bmatrix} \begin{bmatrix} x_1'' \\ x_2'' \end{bmatrix} + \begin{bmatrix} 2D_0 & 0 \\ 0 & 2D \end{bmatrix} \begin{bmatrix} x_1' \\ x_2' \end{bmatrix} + \begin{bmatrix} 1+\gamma & -\gamma \\ -1 & 1+\delta \end{bmatrix} \begin{bmatrix} x_1 \\ x_2 \end{bmatrix} = \begin{bmatrix} \tilde{F}(\tau) \\ 0 \end{bmatrix}. \tag{16}$$

Here, D_0 is the damping ratio, λ is proportional to the external inductance, D proportional to the external resistance and δ proportional to the reciprocal of the external capacitance as given in Eq. (13). All parameters used are positive or equal to zero, apart from the parameter δ which is negative for a negative capacitance. A stability analysis based on Eq. (16) has been performed using the Hurwitz criterion. It can be shown that the system with positive values of resistance and inductance is asymptotically stable for

$$\delta > \delta_{\text{crit}} = -\frac{1}{1+\gamma}. \tag{17}$$

The effect of an external capacitance is highlighted in Fig. 2. A positive capacitance is represented by a spring with positive stiffness c_δ connected between the absorbing mass m_p and the ground. Therefore it reduces the vibration amplitudes of this mass and decreases the absorbing and damping effect. Using a negative capacitance results in a spring with a negative stiffness. It is an active element that amplifies the vibration amplitudes of the

absorbing mass and therefore increases the energy dissipation in the damping element. Eq. (16) describes the most general case of a LRC-network in serial configuration. Having these equations, it is easy to derive the equations for the more common cases of resistance only (case 1) and resistance and inductance (case 2) networks by setting the parameters λ and δ (case 1) resp. δ only (case 2) equal to zero. In all following sections, an undamped mechanical system is assumed by setting the parameters d_0 and D_0 equal to zero.

4. L-network

By setting the parameters δ and D equal to zero (resp. $R = 0$ and $C \to \infty$), a system containing a L-network can be studied. The corresponding mechanical replacement model is given in Fig. 2 when removing the spring c_δ and the damper d_{sd}. The resulting model is the most common mechanical system used for absorbing. The equations of motion read

$$\begin{bmatrix} 1 & 0 \\ 0 & \lambda \end{bmatrix} \begin{bmatrix} x_1'' \\ x_2'' \end{bmatrix} + \begin{bmatrix} 0 & 0 \\ 0 & 0 \end{bmatrix} \begin{bmatrix} x_1' \\ x_2' \end{bmatrix} + \begin{bmatrix} 1+\gamma & -\gamma \\ -1 & 1 \end{bmatrix} \begin{bmatrix} x_1 \\ x_2 \end{bmatrix} = \begin{bmatrix} \tilde{F}(\tau) \\ 0 \end{bmatrix}. \tag{18}$$

Here, the damping matrix is reduced to a matrix of zeros indicating that no energy is dissipated. The FRF-function $V(\eta)$ is given as

$$V(\eta) = \frac{\lambda\eta^2 - 1}{\lambda\eta^4 - (\lambda + \gamma\lambda + 1)\eta^2 + 1}. \tag{19}$$

The absorbing frequency of this system can be determined as

$$\eta_{\text{abs}} = \sqrt{\frac{1}{\lambda}}, \tag{20}$$

while the two resonances are located at

$$\eta_{\text{res1,2}} = \sqrt{\frac{1}{2}\left(1 + \gamma + \frac{1}{\lambda} \pm \sqrt{1 + 2\gamma\left(1 + \frac{1}{\lambda}\right) + \gamma^2 - \frac{2}{\lambda} + \frac{1}{\lambda^2}}\right)}. \tag{21}$$

When setting $\lambda = 1$, which means $\eta_{\text{abs}} = 1$, the equations for the resonance frequencies are as follows,

$$\eta_{\text{res1,2}} = \sqrt{1 + \frac{\gamma}{2} \pm \sqrt{\gamma + \frac{\gamma^2}{4}}}. \tag{22}$$

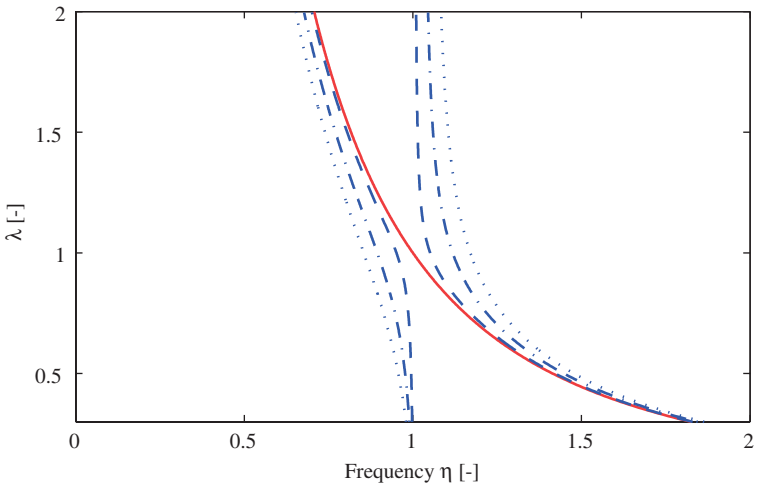

Fig. 3. Absorbing frequency (—), resonance frequencies: (- - -), (-·-·-), (· · · · · ·) for $\gamma = 0.01/0.05/0.10$ versus inductance λ.

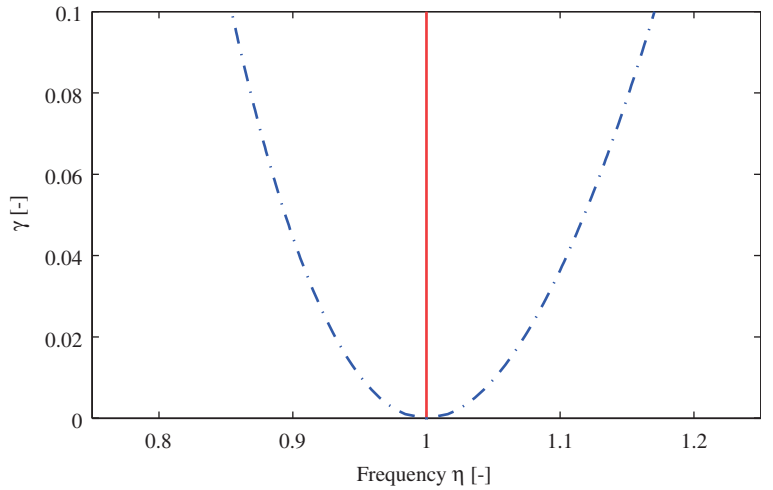

Fig. 4. Absorbing frequency (—) and resonance frequencies (-·-·-) for $\lambda = 1$ versus γ.

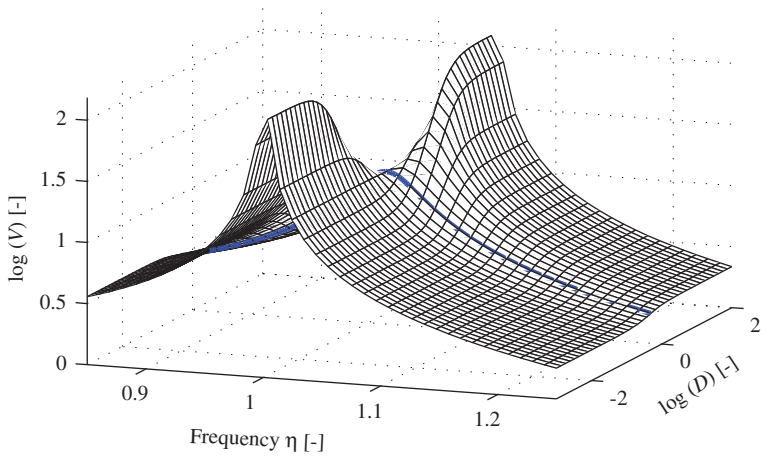

Fig. 5. FRF for R-network, parameter D varied; optimum D marked by thick line.

Both equations show that the difference between the resonance frequencies is increasing with γ, resulting in a broader absorbing area. The absorbing and resonance frequencies are given in Figs. 3 and 4a versus λ resp. γ. As the coupling coefficient of piezo elements usually ranges around 10% [5], the absorbing area is very limited making this network only usable for systems excited by a very steady frequency.

5. R-network

By setting the parameters λ and δ in the general case of the LRC-network in Eq. (16) to zero, the following equations are derived:

$$\begin{bmatrix} 1 & 0 \\ 0 & 0 \end{bmatrix} \begin{bmatrix} x_1'' \\ x_2'' \end{bmatrix} + \begin{bmatrix} 0 & 0 \\ 0 & 2D \end{bmatrix} \begin{bmatrix} x_1' \\ x_2' \end{bmatrix} + \begin{bmatrix} 1+\gamma & -\gamma \\ -1 & 1 \end{bmatrix} \begin{bmatrix} x_1 \\ x_2 \end{bmatrix} = \begin{bmatrix} \tilde{F}(\tau) \\ 0 \end{bmatrix}. \tag{23}$$

The resistance network can be used for vibration damping only, as there is no resonant network which is required for absorbing. The corresponding FRF is shown in Fig. 5. As for all other figures shown in this paper, a value of $\gamma = 0.1$ is assumed, if not mentioned explicitly. This is a rather high value unlikely to happen

in applications, but the properties of the function are distinctive. The case of short-circuit electrodes is represented by $D = 0$, and the open electrodes by $D \to \infty$. The resonance for the first case is located at $\eta = 1$, while the resonance for open electrodes is at $\eta = \sqrt{1+\gamma}$. Here the property of a piezo element to change its stiffness from open to short-circuit electrodes can be observed, which results in a shifted resonance frequency. Another property of this function is the existence of a fixpoint located at

$$\eta_{\text{fix}} = \sqrt{1 + (1/2)\gamma} \tag{24}$$

at which the amplitudes for any value of D are equal. A reasonable criterion for the optimal external resistance for damping is to minimize the largest appearing amplitude of the FRF. Here, the existence of the above-mentioned fixpoint can be used. For the optimal resistance, this fixpoint has to become a maximum. This leads to the following expression,

$$\left.\frac{\partial V(D = D_{\text{opt}})}{\partial \eta}\right|_{\eta=\eta_{\text{fix}}} = 0. \tag{25}$$

The optimal resistance can then be obtained as

$$D_{\text{opt}} = \sqrt{\frac{1}{4+2\gamma}}, \tag{26}$$

with a maximum amplitude of

$$V_{\max} = \frac{2}{\gamma}. \tag{27}$$

Again, a larger value of the coupling coefficient γ leads to a better damping performance.

6. LR-network

A network consisting of resistive and inductive elements can be used for absorbing as well as for damping depending on the resistance used. For absorbing, it is best to have a very small value for D, i.e. a network including an inductance only. The additional resistance leads to a reduction of the resonance amplitudes, but also decreases the absorbing effect. For a certain range of resistance, the FRF-function of the system does not show any significant resonance magnification anymore. This relation of inductance and resistance can be used for broadband damping. The equations are derived below, and a comparison shows that the damping performance of such LR-network is much superior compared to the R-network. A resistance higher than that optimal value leads to open electrodes' behavior of the system with strong resonance amplification again. As before, the equations of motion for the LR-case can be derived from Eq. (16) by setting δ equal to zero,

$$\begin{bmatrix} 1 & 0 \\ 0 & \lambda \end{bmatrix} \begin{bmatrix} x_1'' \\ x_2'' \end{bmatrix} + \begin{bmatrix} 0 & 0 \\ 0 & 2D \end{bmatrix} \begin{bmatrix} x_1' \\ x_2' \end{bmatrix} + \begin{bmatrix} 1+\gamma & -\gamma \\ -1 & 1 \end{bmatrix} \begin{bmatrix} x_1 \\ x_2 \end{bmatrix} = \begin{bmatrix} \tilde{F}(\tau) \\ 0 \end{bmatrix}. \tag{28}$$

For every $\lambda > 0$, this function has two fixpoints, where the amplitudes are not depending on D. For an optimal damping design, the amplitudes at these fixpoints should be equal [5]. It can be shown, that this is achieved be tuning the absorbing frequency to the resonance frequency with open electrodes. This leads to the following relation for λ,

$$\lambda_{\text{opt}} = \frac{1}{1+\gamma}. \tag{29}$$

The fixpoints then are located to the left and to the right of the resonance frequency for open electrodes at the frequencies

$$\eta_{\text{fix1,2}} = \sqrt{1 + \gamma \pm \frac{1}{\sqrt{2}}\sqrt{\gamma + \gamma^2}}, \tag{30}$$

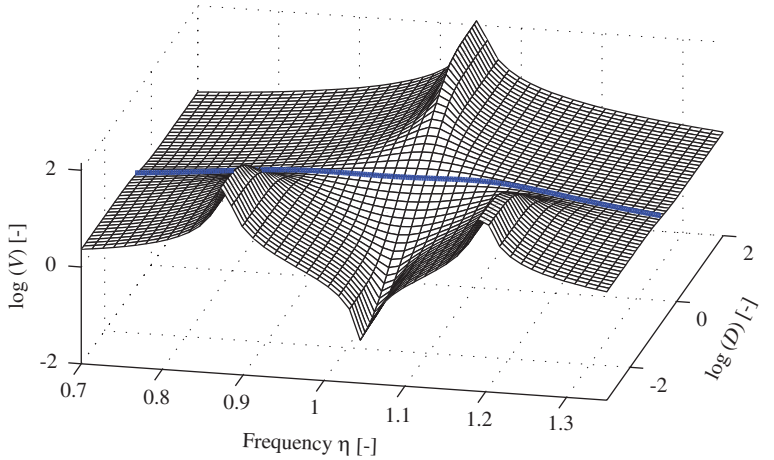

Fig. 6. FRF for LR-network, parameter D varied; optimum D marked by thick line.

having the same amplitude

$$V(\eta = \eta_{\text{fix}}) = \sqrt{\frac{2}{\gamma + \gamma^2}}. \tag{31}$$

This result again shows that a high value of γ decreases the amplitudes. For such an inductance, the amplitude for $\eta = \eta_{\text{res}}$ is strictly monotonic increasing with larger resistance from $V(\eta = \eta_{\text{res}}) = 0$ for $D = 0$ (absorbing) to $V(\eta = \eta_{\text{res}}) \to \infty$ for $D \to \infty$ (open electrodes),

$$V(\eta = \eta_{\text{res}}) = 2D\frac{\sqrt{1+\gamma}}{\gamma}. \tag{32}$$

That resistance, for which this amplitude is equal to the amplitude at the fixpoints is commonly stated as the optimal resistance,

$$D_{\text{opt}} = \sqrt{\frac{1}{2/\gamma + 4 + 2\gamma}}. \tag{33}$$

A comparison of Eqs. (26) and (33) shows that the optimal resistance for a LR-network is smaller than for a R-network. Fig. 6 shows the FRF of the LR-network with optimal inductance and resistance varied. The absorbing area is present for small values of resistance and is surrounded by two resonances. The optimum resistance equalizes the amplitudes of the fixpoints and of the resonance frequency for the system with open electrodes, which leads to a flat FRF with a minimized maximum amplitude but also no absorbing area. This line is also shown in Fig. 6.

7. Comparison of R- and LR-networks

In this section, the optimal tuned R- and LR-networks are compared. The result is depicted in Fig. 7. The optimal lines for both kinds of networks are plotted versus parameter γ. The FRF for the optimal R-network has one strong resonance frequency. It is clearly noticeable that the damping effect is increased for higher values of γ. In contrast to this, the optimal LR-network does not show any noticeable resonance amplification. The overall function is more flat and the better damping performance of the LR-network is evident. However, for very small and very high frequencies, the R-network has the slightly smaller amplitudes.

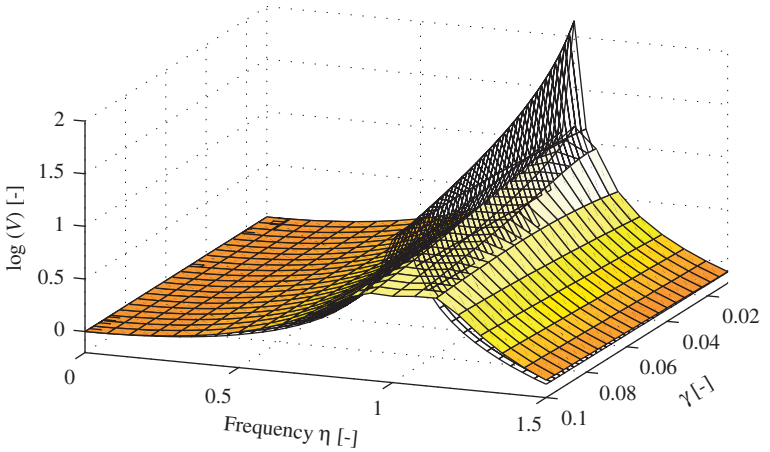

Fig. 7. Damping performance for optimum LR- (surface) and R- (wire frame) network versus parameter γ.

8. C-networks

After concluding the passive networks, in this section the effect of a network consisting only of a negative capacitance is studied, before analyzing general networks containing passive and semi-active elements in the following sections. It is known and experimentally verified [6] that a negative capacitance shunted to a piezoelectric transducer is capable of changing the elasticity of the piezo element. When the piezo element is the dominating system stiffness, this directly leads to a shifting of the resonance frequency. Setting the values for resistance and inductance to zero, one gets the following equations of motion,

$$\begin{bmatrix} 1 & 0 \\ 0 & 0 \end{bmatrix} \begin{bmatrix} x_1'' \\ x_2'' \end{bmatrix} + \begin{bmatrix} 1+\gamma & -\gamma \\ -1 & 1+\delta \end{bmatrix} \begin{bmatrix} x_1 \\ x_2 \end{bmatrix} = \begin{bmatrix} \tilde{F}(\tau) \\ 0 \end{bmatrix}, \tag{34}$$

with the external capacitance described by parameter $\delta = C_{ps}/C$. The second equation describes the relation between x_1 and x_2,

$$x_2 = \frac{x_1}{1+\delta}, \tag{35}$$

which can be inserted into the first equation resulting in

$$x_1'' + \left(\frac{1+\delta+\gamma\delta}{1+\delta}\right) x_1 = \tilde{F}(\tau). \tag{36}$$

In this normalized form, the resonance frequency can easily be obtained as

$$\eta_{\text{res}} = \sqrt{\frac{1+\delta+\gamma\delta}{1+\delta}}. \tag{37}$$

A plot is shown in Fig. 8. Studying Eq. (37) one can derive the effect of positive and negative capacitances. By positive capacitances, which means $\delta > 0$, the resonance frequency can be shifted in the range $1 \leqslant \eta_{\text{res}} \leqslant \sqrt{1+\gamma}$, which are the resonance frequencies for open- and short-circuit electrodes. For a common value of γ a maximum frequency shift of about 0.5% can be achieved. When applying a negative capacitance, the resonance frequency can (theoretically) be shifted to any frequency apart from that range. Decreasing the parameter δ from $\delta = 0$ towards $\delta = -1/(1+\gamma)$ reduces the resonance frequency from 1 towards zero, cf. Fig. 8. When increasing δ from $-\infty$ towards -1 (which means decreasing the real value C from 0 towards $-C_{ps}$), the resonance frequency is shifted from $\eta_{\text{res}} = \sqrt{1+\gamma}$ towards $\eta_{\text{res}} \to \infty$. In the range

$$-1 < \delta < -\frac{1}{1+\gamma} \tag{38}$$

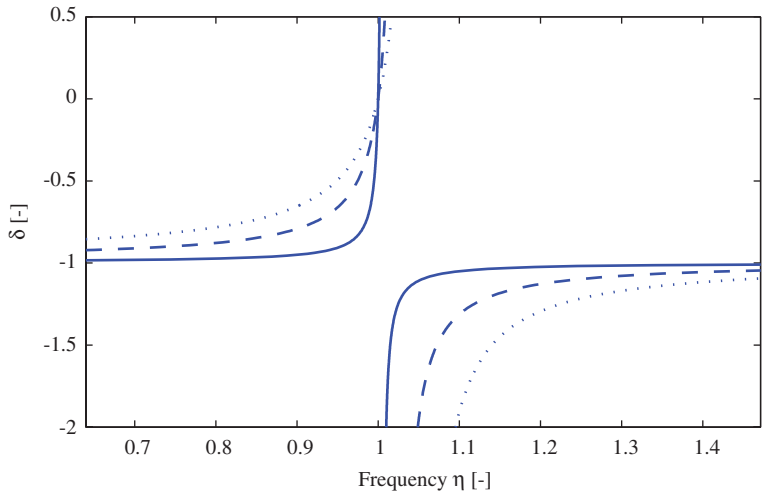

Fig. 8. Resonance frequencies: (—), (- - -), (·····) versus δ for $\gamma = 0.01/0.05/0.10$.

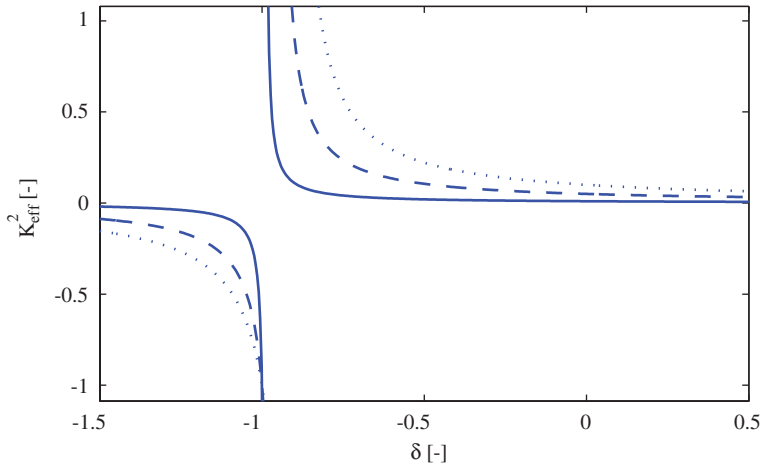

Fig. 9. Square of effective coupl. coeff. K: (—), (- - -), (·····) versus δ for $\gamma = 0.01/0.05/0.10$.

the system is unstable. This range has to be excluded. For $\delta = 0$ the resonance frequency is located at $\eta_{res} = 1$ for any value of γ. This is the case of short-circuit electrodes. With the resonance frequencies given in Eq. (37), where the resonance for open electrodes remains constant at $\eta_{res} = \sqrt{1+\gamma}$, the apparent electromechanical coupling coefficient can be derived. The definition according to Eq. (15) leads to

$$K_{eff}^2 = \frac{(1+\gamma)(1+\delta)}{1+\delta+\gamma\delta} - 1. \tag{39}$$

Fig. 9 shows a plot of the apparent coupling coefficient K_{eff} versus parameter δ for different values of γ. Per definition $\delta = 0$ results in $K_{eff} = \sqrt{\gamma}$. The graphs shows that the coupling coefficient is generally increased by negative capacitances. For δ close to the critical value δ_{crit} according to Eq. (17), the coupling coefficient increases nearly instantly towards infinity. This effect is even increased for small values of γ. This means that theoretically the coupling coefficient can be increased for any value of γ, but practically tuning is difficult for small values of γ because of the high sensitivity regarding changes of δ. Beyond this critical value, the square of the coupling coefficient gets negative, that is physically not meaningful, and the system becomes unstable.

9. LC-network

In this section a network consisting of inductance and capacitance is studied. The LC-network includes the special case of the L-network, which results from setting the parameter δ equal to zero. The equations for the LC-network reads

$$\begin{bmatrix} 1 & 0 \\ 0 & \lambda \end{bmatrix} \begin{bmatrix} x_1'' \\ x_2'' \end{bmatrix} + \begin{bmatrix} 1+\gamma & -\gamma \\ -1 & 1+\delta \end{bmatrix} \begin{bmatrix} x_1 \\ x_2 \end{bmatrix} = \begin{bmatrix} \tilde{F}(\tau) \\ 0 \end{bmatrix}. \tag{40}$$

The resulting system has in analogy to the L-network two resonances and one absorbing frequency. The effect of the external capacitance C (i.e. δ) is a change in the resonance frequency of the network and therefore of the absorbing frequency. This frequency can be calculated as

$$\eta_{\text{abs}} = \sqrt{\frac{1+\delta}{\lambda}} = \sqrt{1+\delta}\,\eta_{\text{abs},L}. \tag{41}$$

The two resonance frequencies are located at

$$\eta_{\text{res}} = \sqrt{\frac{1}{2}\left(1+\gamma+\frac{1+\delta \pm \sqrt{(1+\gamma)^2\lambda^2 + 2[(1-\delta)\gamma-(1+\delta)]\lambda + (1+\delta)^2}}{\lambda}\right)}. \tag{42}$$

These frequencies are plotted in Fig. 10. The required inductance λ to absorb a certain frequency is therefore changed in the following way:

$$\lambda = (1+\delta)\lambda_L, \tag{43}$$

with the constant absorbing frequency

$$\eta_{\text{abs}} = \sqrt{\frac{1+\delta}{\lambda}} = \sqrt{\frac{1+\delta}{(1+\delta)\lambda_L}} = \sqrt{\frac{1}{\lambda_L}}, \tag{44}$$

where λ_L is the required inductance for the L-network only ($\delta = 0$). When setting $\eta_{\text{abs}} = 1$ which means that $\lambda_L = 1$ and $\lambda = 1+\delta$, the resonance frequencies are as follows

$$\eta_{\text{res1,2}} = \sqrt{1+\frac{\gamma}{2} \pm \sqrt{\frac{\gamma}{1+\delta}+\frac{\gamma^2}{4}}}. \tag{45}$$

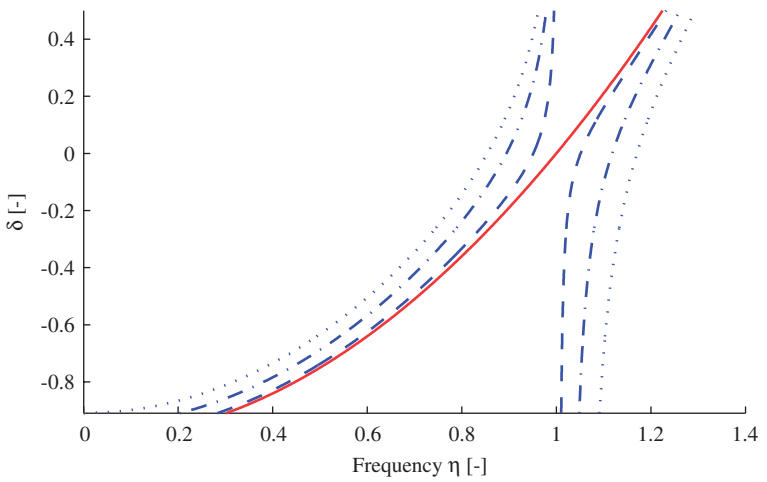

Fig. 10. Absorbing frequency (—) and resonance frequencies: (- - -), (-·-·-), (·····) of the LC-network versus δ for $\gamma = 0.01/0.05/0.10$.

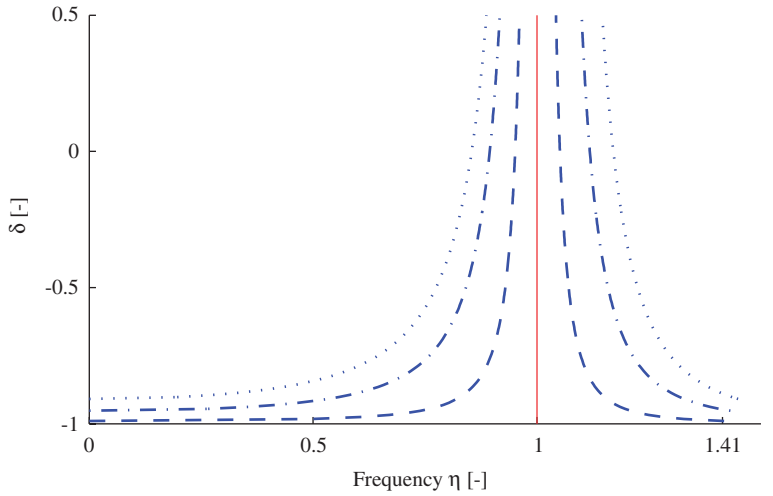

Fig. 11. Absorbing frequency (—) and resonance frequencies: (- - -), (-·-·-), (·····) of the LC-network versus δ for $\gamma = 0.01/0.05/0.10$ for a constant absorbing frequency.

With the absorbing frequency not depending on δ, the difference of the two resonance frequencies is increased with a negative capacitance, leading to an increased absorbing area, cf. Fig. 11. That means a negative capacitance has a similar effect as an increase of the electromechanical coupling coefficient. The maximum possible effect of increasing the absorbing area is achieved when tuning δ exactly to stability boundary $\delta_{\text{crit}} = -1/(1+\gamma)$ as given in Eq. (17). With Eq. (42) it follows

$$\begin{aligned} \eta_{\text{res1,crit}} &= 0, \\ \eta_{\text{res2,crit}} &= \sqrt{1+\gamma+\gamma/(1+\gamma)\lambda}\,. \end{aligned} \tag{46}$$

It is of practical relevance how the resonances can be shifted while absorbing a given frequency η_{abs}. Depending on the absorbing frequency, the resonance frequencies for $\delta = \delta_{\text{crit}}$ are

$$\begin{aligned} \eta_{\text{res1,crit}} &= 0, \\ \eta_{\text{res2,crit}} &= \sqrt{1+\eta_{\text{abs}}^2+\gamma}\,. \end{aligned} \tag{47}$$

Considering the parameter γ to be relatively small ($\gamma \approx 1\%$ when $K_{3i} = 0.1$ for typical applications), the maximum possible spreading of the resonances when tuning to $\delta = \delta_{\text{crit}}$ results in $\eta_{\text{res2,crit}} \approx \sqrt{1+\eta_{\text{abs}}^2}$. This means the maximum possible absorbing effect is nearly independent from the parameter γ but tuning is more difficult with γ.

10. RC-network

Next, RC-networks are discussed. Criteria for optimal tuning of resistance and inductance will be given, and the resulting damping performance is compared to R-networks. As already mentioned, cf. Eq. (17), a negative capacitance is capable of destabilizing the system when tuned close to the negative value of piezoelectric capacitance. These limitations are always regarded in the following sections.

The equations of motion for the RC-network read

$$\begin{bmatrix} 1 & 0 \\ 0 & 0 \end{bmatrix} \begin{bmatrix} x_1'' \\ x_2'' \end{bmatrix} + \begin{bmatrix} 0 & 0 \\ 0 & 2D \end{bmatrix} \begin{bmatrix} x_1' \\ x_2' \end{bmatrix} + \begin{bmatrix} 1+\gamma & -\gamma \\ -1 & 1+\delta \end{bmatrix} \begin{bmatrix} x_1 \\ x_2 \end{bmatrix} = \begin{bmatrix} \tilde{F}(\tau) \\ 0 \end{bmatrix}. \tag{48}$$

For every value of the capacitance δ there exists again a fixpoint, where all FRFs independent of the resistance are crossing, located at

$$\eta_{\text{fix}} = \sqrt{\frac{1 + (\gamma/2) + \delta + \gamma\delta}{1 + \delta}}, \tag{49}$$

cf. Eq. (24). In analogy to the R-network, the resistance is tuned in such a way that this fixpoint coincides with the maximum amplitude for all frequencies. This leads to the following result for the optimal damping:

$$D_{\text{opt}} = \sqrt{\frac{(1+\delta)^3}{4 + 2\gamma + 4\delta(1+\gamma)}}. \tag{50}$$

The amplitude at the fixpoint is given by

$$V(\eta = \eta_{\text{fix}}) = \frac{2 + 2\delta}{\gamma}. \tag{51}$$

It can be observed that the amplitude of the fixpoint is monotonic decreasing with negative values of δ down to $V(\eta = \eta_{\text{fix}}) = \sqrt{(1+\gamma)/2}$ for the stability boundary at $\delta_{\text{crit}} = -1/(1+\gamma)$. On the other hand the static displacement for $\eta = 0$ is magnified by a negative capacitance,

$$V(\eta = 0) = \frac{1 + \delta}{1 + \delta + \gamma\delta}. \tag{52}$$

As defined by normalizing the equations, $V(\eta = 0) = 1$ for $\delta = 0$. So, by a negative capacitance, the amplitude of the fixpoint is decreased while the static displacement is increased. The optimal value for negative capacitance, which minimizes the overall maximum amplitude, can therefore be obtained by equating both amplitudes. For values of δ larger than this optimal value, the maximum amplitude appears at the fixpoints, for smaller values the static displacement at $\eta = 0$ is the maximum. This criterion results in the following equation for δ_{opt},

$$\delta_{\text{opt}} = \frac{\gamma/2 - 1}{\gamma + 1}. \tag{53}$$

Interestingly, the optimal value for δ does not correspond to the stability boundary of the system at δ_{crit}.

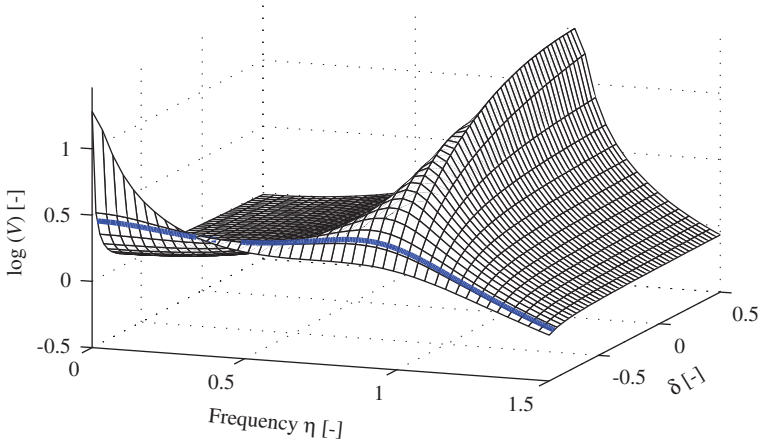

Fig. 12. FRF for optimum RC-network versus δ; optimum δ marked by thick line.

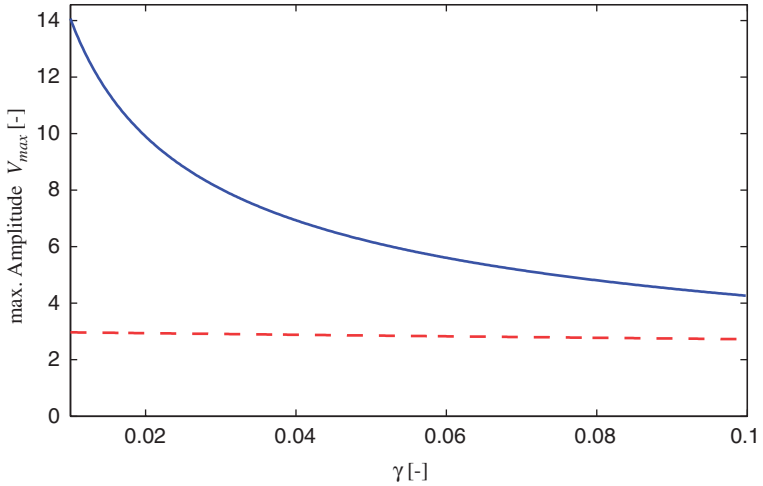

Fig. 13. Max. amplitudes for opt. LR- (—) and opt. RC- (- - -) networks.

The corresponding optimal resistance is derived by substituting this value into Eq. (50). The maximum amplitude of the FRF with optimal tuned RC-network reads

$$V_{\max} = \frac{3}{1+\gamma}. \tag{54}$$

Fig. 12 shows the FRFs of optimal tuned RC-networks versus δ. The line for optimal δ is marked by a thick line. Consider that the optimal R-network without negative capacitance is given at $\delta = 0$. It is evident that the damping effect is increased significantly when using a negative capacitance, being maximized for $\delta = \delta_{\text{opt}}$. As presumed and confirmed by Eq. (54), a larger value of γ leads to a better damping performance. It supersedes optimal passive networks for any value of γ possible in real applications. But unlike for passive R- and LR-networks, the influence of γ upon the damping performance is relatively small, i.e. that even with a small value of γ good damping performance is achievable, cf. Fig. 13. Moreover, an upper limit for the maximum amplitude can be given by $V_{\max} = 3$. But, as can be seen from Eq. (53), negative capacitance has to be tuned closer to the stability boundary for small γ, which means, the system is very sensitive for small changes of δ-values.

11. LRC-network

The following calculations are performed in an analogical way as for the LR-network for damping and the same criteria are used to find the optimized parameters. Starting with the equations of motion,

$$\begin{bmatrix} 1 & 0 \\ 0 & \lambda \end{bmatrix} \begin{bmatrix} x_1'' \\ x_2'' \end{bmatrix} + \begin{bmatrix} 0 & 0 \\ 0 & 2D \end{bmatrix} \begin{bmatrix} x_1' \\ x_2' \end{bmatrix} + \begin{bmatrix} 1+\gamma & -\gamma \\ -1 & 1+\delta \end{bmatrix} \begin{bmatrix} x_1 \\ x_2 \end{bmatrix} = \begin{bmatrix} \tilde{F}(\tau) \\ 0 \end{bmatrix} \tag{55}$$

one can see they differ only by the term $(1+\delta)$ in the stiffness matrix from the equations for the LR-case, cf. Eq. (28). The resonance frequency for open electrodes again lies at $\eta_{\text{res}} = \sqrt{1+\gamma}$, while the absorbing frequency is located at $\eta_{\text{abs}} = \sqrt{(1+\delta)/\lambda}$. Again the effect of a decreased absorbing frequency by a negative capacitance can be observed. The optimal value is calculated in the same way as for LR-network by equating the frequencies of absorbing and resonance for open electrodes, cf. Eq. (29). This results in

$$\lambda_{\text{opt}} = \frac{1+\delta}{1+\gamma} \rightarrow \lambda_{\text{opt}} = (1+\delta)\lambda_{\text{opt},LR}. \tag{56}$$

It can be shown that a negative value for δ leads to a reduction of the required value for λ (resp. inductance), compensating the effect of decreased absorbing frequency by the negative capacitance, while the resonance for open electrodes does not change. For such a parameter-constellation, the fixpoints are located at

$$\eta_{\mathrm{fix1,2}} = \sqrt{1+\gamma \pm \frac{1}{\sqrt{2}}\sqrt{\frac{\gamma^2+\gamma}{1+\delta}}}. \tag{57}$$

This equation shows clearly the effect of spreading the fixpoints by a negative capacitance δ. The amplitude at the resonance frequency is $V(\eta_{\mathrm{res}}) = 2D\sqrt{(1+\gamma)}/\gamma$, while the amplitudes at the fixpoints are $V(\eta_{\mathrm{fix}}) = \sqrt{2(1+\delta)/(\gamma^2+\gamma)}$. This term shows a reduction of the amplitudes for a negative value of δ. The criterion for optimal parameter D is to equate these amplitudes,

$$D_{\mathrm{opt}} = \sqrt{\frac{1+\delta}{2/\gamma+4+2\gamma}} = \sqrt{1+\delta}\,D_{\mathrm{opt},LR}. \tag{58}$$

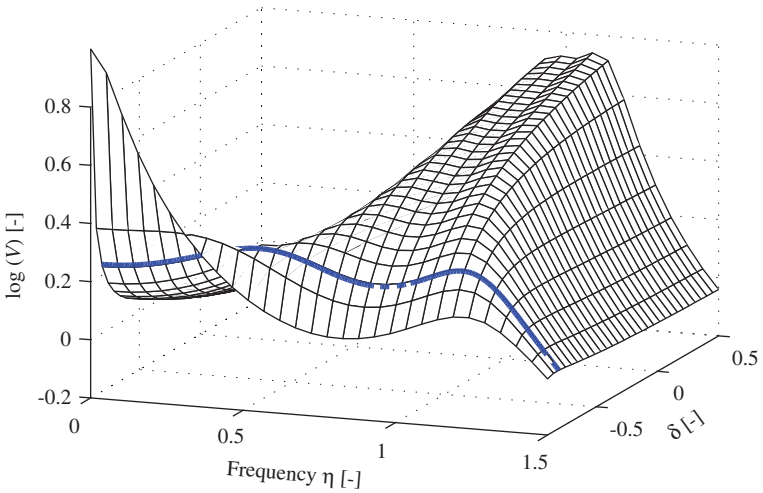

Fig. 14. FRF for optimum LRC-network versus δ; optimum δ marked by thick line.

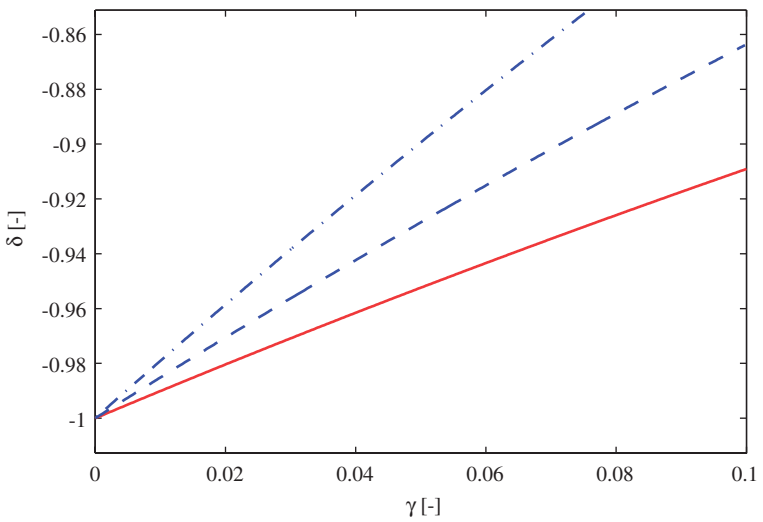

Fig. 15. δ_{crit} (—), δ_{opt} (-·-·-) for LRC- and δ_{opt} (- - -) for RC-networks versus γ.

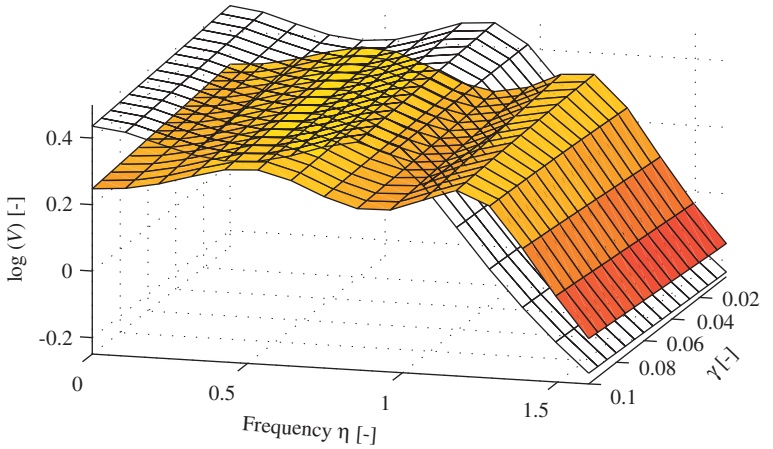

Fig. 16. Damping performance for optimum LRC- (surface) and RC-(wire frame) networks versus γ.

Eqs. (56) and (58) clearly indicate the reduced values for resistance and inductance for the optimal LRC-network compared to the optimal LR-network.

As already mentioned by Tang and Wang [5] the usually quite small piezoelectric capacitance leads to a large optimal inductance for the LR-network, which probably has to be built synthetically. A negative capacitance can therefore make the synthetic inductor unnecessary.

The amplitudes for optimal damping according to Eq. (58) are depicted in Fig. 14 versus parameter δ. One can see that generally a negative capacitance leads to better damping, as presumed before. Consider the line at $\delta = 0$ is the line of optimal damping for the LR-network. As in the case of the RC-network, there again exists an optimal value δ_{opt} which minimizes the maximum amplitude,

$$\delta_{\text{opt}} = \frac{\gamma k_{LRC} - 1}{\gamma + 1}, \quad k_{LRC} = \frac{\sqrt{17}}{2}\cos\left(\frac{\text{arcustangens}\,(4)}{3}\right) - \frac{3}{4} \approx 1.113, \tag{59}$$

which has the same form as δ_{opt} for the RC-network, for which $k_{RC} = 0.5$, cf. Eq. (53). The corresponding frequency response function is highlighted in Fig. 14 by a thick line. Again a smaller value of γ results in δ_{opt} closer to $\delta = -1$ which means closer to the stability boundary of the system. For the parameter as shown in Fig. 14, δ_{opt} is calculated as $\delta_{\text{opt}} = -0.808$. The optimal parameter δ_{opt} for RC- and LRC-networks and the stability boundary δ_{crit}, which is the same for both kind of networks, are plotted in Fig. 15 versus parameter γ. The difference between δ_{crit} and δ_{opt}, which can be treated as the safety margin to the stability boundary is given as

$$\delta_{\text{opt}} - \delta_{\text{crit}} = \frac{k\gamma}{1 + \gamma}, \quad k = k_{LRC} \quad \text{resp. } k = k_{RC}. \tag{60}$$

It is larger for the LRC-network than for the RC-network, and it is growing for larger values of γ for both networks, which makes the tuning to the optimal values easier. A comparison of optimal tuned RC-network according to Eqs. (50) and (53) and the optimal tuned LRC-network according to Eqs. (56) and (58) is given in Fig. 16 versus parameter γ. Unlike in passive networks, amplitudes for small values of γ are only slightly higher than for large values of γ. The damping performance of LRC-networks is yet superior to RC-networks, the upper limit for the maximum amplitude can be given as

$$\lim_{\gamma \to 0} V_{\max} = 2.38, \tag{61}$$

compared to $V_{\max} = 3$ for the RC-network. Also the static displacement for the optimal RC-network is larger than for the LRC-network, because $\delta_{\text{opt},RC}$ is closer to -1 than $\delta_{\text{opt},LRC}$. For both semi-active networks, the static displacement is larger than the normalized static amplitude of passive networks, $V(\eta = 0) = 1$.

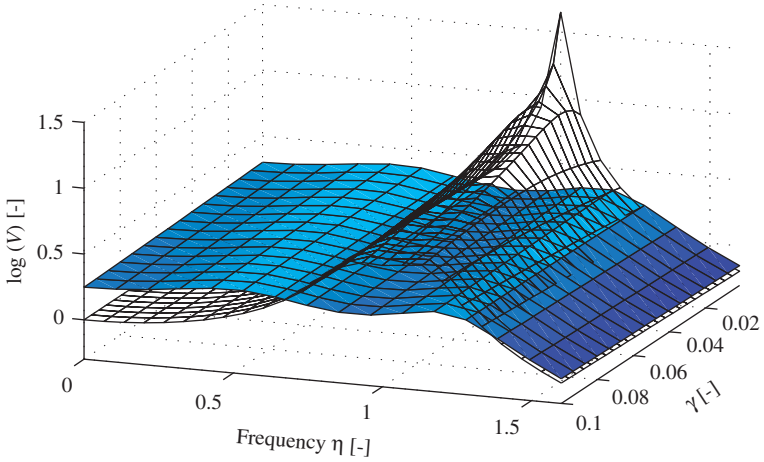

Fig. 17. Damping performance for optimum LRC- (surface) and LR-(wire frame) networks versus γ.

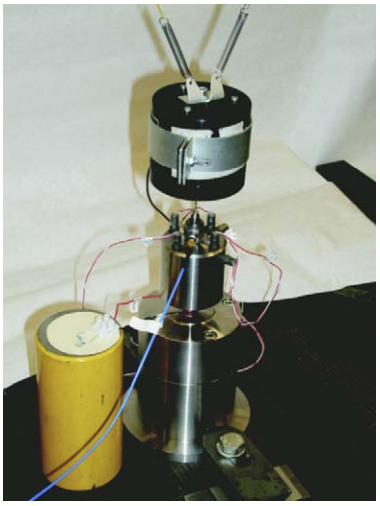

Fig. 18. Test rig.

12. Comparison of optimal passive and semi-active networks

The analytical discussion of passive and semi-active networks concludes in a comparison of both methods. Best damping performance in passive systems can be achieved by LR-networks, cf. Fig. 7, while LRC-networks result in the best semi-active constellation, cf. Fig. 16. A comparison of these damping performances gives insight how much potential for improvement is given with semi-active networks, cf. Fig. 17. It can be seen that the addition of the optimal negative capacitance reduces the maximum amplitudes in the FRF significantly, thus increasing the damping performance of the system. The overall FRF is very flat, but for small frequencies (especially for $\eta = 0$), the amplitudes are larger than for passive networks, caused by the negative capacitance reducing the effective stiffness of piezo element. Also for high frequencies the amplitudes of the LRC-network are slightly larger than of the LR-network. While damping performance of LR-networks is diminished significantly for small γ, damping performance of optimal LRC-networks shows only little influence of this parameter. Thus, the improvement in performance caused by an additional negative capacitance is better, the smaller the parameter γ. These results are based on the assumption that optimal tuning is possible and the operational

amplifiers in synthetic negative capacitance always generate the required voltage, which is proportional to the amplitudes of excitation forces.

13. Measurements

Experimental investigations have been performed with different configurations of impedance shunt circuits. The aim is to validate the analytical results and to prove the increased damping and absorbing performance for optimum LRC-networks compared to optimum LR-networks predicted by the analytical investigations shown before. The test rig consists of a vibration mass of 1.1 kg which is mounted on top of a piezoelectric stack actuator, cf. Fig. 18. The piezo element used is a tubular HVPZT stack translator PI-305 (Physics Instruments). The synthetic negative capacitance circuit was realized with a single high-voltage OPA445 operational amplifier as an impedance converter, based on Ref. [7]. Negative capacitance was gained by changing the amplification factor of the operational amplifier. The positive capacitance value in the circuit is 22 nF. For symmetric supply, voltage of ±40 V has been applied, the overall power consumption was less than 0.3 W. The stiffness c_{33} of the piezo element is calculated from the measured mass and eigenfrequency for short-circuit electrodes. The maximum normal pressure of the piezo element is limited to 500 N. In order to use the maximum possible vibration amplitude, a pre-stress of 250 N has been applied to the piezo element by an additional spring c_0 which is connected between the mass and the base.

The absorbing frequency was tuned equal to the resonance frequency for open electrodes as suggested in the section L-network to achieve maximum damping performance. Using an inductance of $L_0 = 640\,\text{mH}$ the absorbing frequency was located at $f_{\text{abs}} = 1625\,\text{Hz}$ with the resonances at $f_{\text{res1}} = 1445\,\text{Hz}$ and $f_{\text{res2}} = 1800\,\text{Hz}$, or normalized according to Eq. (13),

$$\eta_{\text{abs}} = 1.0125, \quad \eta_{\text{res1}} = 0.9003, \quad \eta_{\text{res2}} = 1.1215. \tag{62}$$

The parameter λ_0 is defined by the absorbing frequency, cf. Eq. (20):

$$\lambda_0 = \left(\frac{1}{\eta_{\text{abs}}}\right)^2 = 0.9755.$$

The unknown parameter γ can be obtained by solving Eq. (21) for both left and right resonance frequencies. This results in $\gamma = 0.0502$ for the left resonance and $\gamma = 0.0477$ for the right one. In the following the average value of

$$\gamma = 0.0489$$

is assumed. The generalized coupling coefficient of this application is therefore $K_{3i} = 0.22$. The sensitivity of the piezo element can be derived by Eq. (14) as

$$d_{33} = 2.56\,\text{nm/V}.$$

The properties of the test rig are summarized in Table 1. In Fig. 11 the influence of a negative capacitance in a LC-network for absorbing is compared to a L-network. To observe the strongest absorbing performance, the

Table 1
Test rig parameters

Parameter	Value	Description
m_0	1.1 kg	Vibrating mass
C_{ps}	15 nF	Capacitance of piezo stack
c_{33}	111 MN/m	Stiffness of piezo stack for short-circuit electrodes
d_{33}	2.56 nm/V	Sensitivity of piezo stack
c_0	12.5 kN/m	Additional spring
γ	0.0489	Square of gen. electromechanical coupling coefficient
f_{short}	1605 Hz	Eigenfrequency of the system with short-circuit electrodes

value of negative capacitance in the test rig was set to obtain a value of δ closest to $\delta_{\text{crit}} = -1/(1+\gamma) = -0.95$, cf. Eq. (17), which is the stability boundary of the system. The inductance value was set again, to obtain the absorbing frequency equal to the open electrodes' resonance frequency of the system. As proposed in Eq. (43), the required inductance was reduced, in this case to $L = 90\,\text{mH}$, resp. $\lambda = 0.1372$. Eq. (43) can be used to derive the parameter δ that has been achieved in experiment,

$$\delta = \frac{\lambda}{\lambda_0} - 1 = \frac{L}{L_0} - 1 = -0.86.$$

With $C_{ps} = 15\,\text{nF}$, the actual negative capacitance value was $-17.45\,\text{nF}$. As it is practically difficult to reach the optimum value for δ due to the stability boundary, the damping performance is supposed to be even more improved when tuning closer to δ_{crit}. According to Eq. (42) the resonances of the FRF for the LC-network containing these values for δ, λ and γ are located at

$$\eta_{\text{res1}} = 0.66, \quad \eta_{\text{res2}} = 1.28.$$

From measurement data, the resonances are located at

$$f_{\text{res1}} = 1115\,\text{Hz}, \quad f_{\text{res2}} = 2085\,\text{Hz}, \quad \text{resp.} \quad \eta_{\text{res1}} = 0.69, \quad \eta_{\text{res2}} = 1.30.$$

These results are not only in very good accordance to the predicted frequencies, also the considerably improved absorbing performance of the LC-network compared to the L-network is obvious. The difference in frequency of the two resonances is increased almost 3 times from 355 up to 970 Hz. The corresponding measured FRF for the L- and the LC-network are shown in Fig. 19. The test rig has then been used to verify the improved damping performance of networks containing negative capacitances. The optimal tuned R- and LR-networks are compared with the optimum LRC-network as has been shown in Figs. 7 resp. 17 analytically. The optimum resistance for the R-network according to Eq. (26) and revoking the normalization is given as

$$R_{\text{opt},R} = \frac{2}{C_{ps}}\sqrt{\frac{m}{(c_0 + c_{33})(4 + 2\gamma)}} = 6531\,\Omega.$$

For the optimum LR-network, the inductance is set by tuning the absorbing frequency to the resonance frequency for open electrodes. According to Eq. (33), the optimum resistance is given as

$$R_{\text{opt},LR} = \frac{2}{C_{ps}}\sqrt{\frac{m}{(c_0 + c_{33})(2/\gamma + 4 + 2\gamma)}} = 1970\,\Omega.$$

For the LCR-network, the optimum value for δ assuming $\gamma = 0.0489$ is given as $\delta_{\text{opt}} = -0.905$, cf. Fig. 15. However, the network remains to be tuned to $\delta = -0.86$ which is the closest possible value for the network used

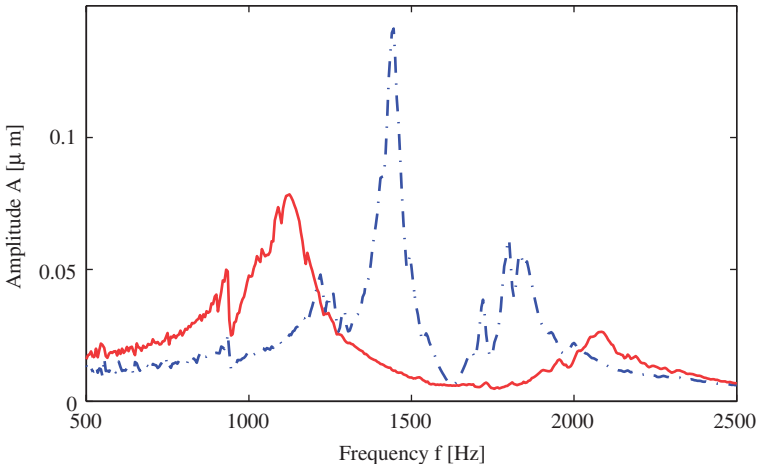

Fig. 19. Measured FRF of LC- (—) and L- (-·-·-) networks; absorbing case.

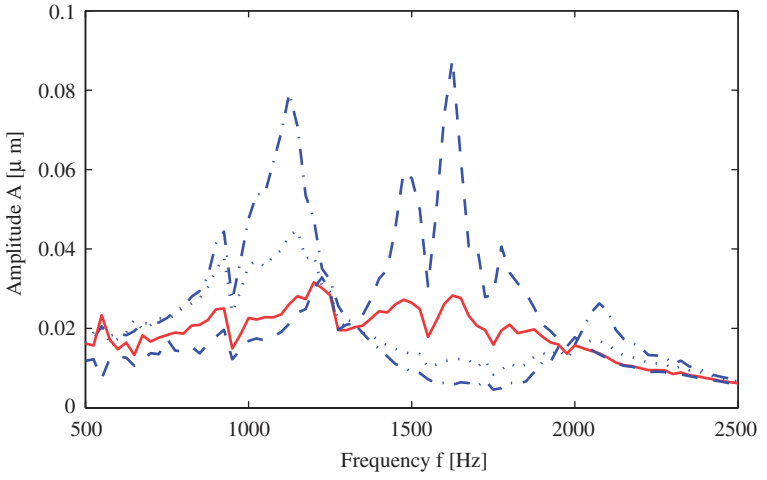

Fig. 20. Measured FRF of LRC-network: (-·-·-), (·····), (- - -): $R = 10/200/5000\,\Omega$; (—): $R = R_{\text{opt}} = 800\,\Omega$.

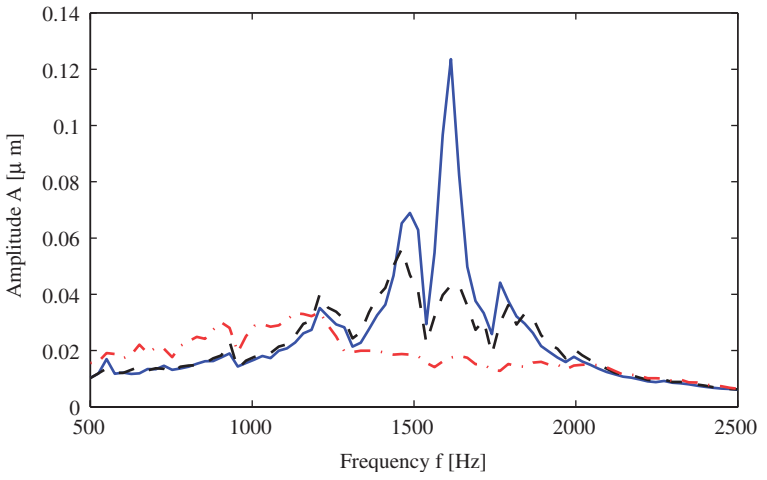

Fig. 21. Measured FRF of opt. R- (—), LR- (- - -) and LRC- (-·-·-) networks.

to emulate a negative capacitance. According to Eqs. (56) and (58), the values for inductance and resistance are decreased

$$L_{\text{opt},LRC} = (1+\delta)L_{\text{opt},LR},$$
$$R_{\text{opt},LRC} = \sqrt{1+\delta}R_{\text{opt},LR} = 739\,\Omega.$$

To prove the existence of the two predicted fixpoints, several FRF with different resistances were measured, keeping the inductance and negative capacitance values constant. The result is shown in Fig. 20. In this graph, the solid line is drawn for the optimum value of resistance according to the proposed criterion. The two fixpoints around which all FRFs meet can clearly be localized at frequencies

$$f_{\text{fix1}} = 1300\,\text{Hz}, \quad f_{\text{fix2}} = 1970\,\text{Hz}, \quad \text{resp.} \quad \eta_{\text{fix1}} = 0.81, \quad \eta_{\text{fix2}} = 1.23.$$

Again, these measured frequencies are in very good accordance with the analytical predictions given by Eq. (57):

$$\eta_{\text{fix1}} = 0.79, \quad \eta_{\text{fix2}} = 1.22.$$

Table 2
Comparison of measurements and analytic predictions

	Analytic result	Measurement
Optimum resistance for R-network $R_{\mathrm{opt},R}$	6531 Ω	6000 Ω
Optimum resistance for LR-network $R_{\mathrm{opt},LR}$	1970 Ω	1500 Ω
Optimum resistance for LRC-network $R_{\mathrm{opt},LRC}$	739 Ω	800 Ω
Left resonance for LC-network $\eta_{\mathrm{res},1}$	0.66	0.69
Right resonance for LC-network $\eta_{\mathrm{res},2}$	1.28	1.30
Left fixpoint for LRC-network $\eta_{\mathrm{fix},1}$	0.79	0.81
Right fixpoint for LRC-network $\eta_{\mathrm{fix},2}$	1.22	1.23

As for the LR-network, it can be seen that the shape of the FRFs change from the absorbing case with two resonances for resistances lower than the optimum value to an open electrodes behavior of the system for resistances larger than the optimum. The optimum line itself has the lowest maximum amplitude of all FRFs.

In Fig. 21, the optimal measured FRFs for R-, LR- and LRC-networks are plotted in one diagram to compare the damping performances of the different networks. The best performances for each network can be achieved using the following resistances:

$$R_R = 6000\,\Omega, \quad R_{LR} = 1500\,\Omega \quad \text{and} \quad R_{LRC} = 800\,\Omega.$$

Especially the resistances used for R- and LRC-networks are very close to the predicted values and prove the proposed criteria. The differences between calculations and measurements are due to the side effects in the test rig, e.g. cables capacitance and reactance losses in the coil used during the experiment. A comparison shows that for passive networks, the LR-network is significantly better in comparison to the R-network. However, the damping performance can still be increased further when using an optimum tuned LRC-network. The maximum appearing amplitude was decreased to 60% compared to the LR-network. This improvement may be further increased when tuning the negative capacitance closer to the proposed optimum value. On the other hand, amplitudes for low frequencies are amplified by the negative capacitance, cf. Fig. 17. The comparison of analytic and measured results is summarized in Table 2.

14. Conclusions

In this paper, a comprehensive study of a negative capacitance in a damping and absorbing system using shunted piezoelectric transducers has been performed. Based on a unifying mechanical model, for each kind of network, criteria for optimal parameters are given and the damping and absorbing performance of these networks tuned to the proposed optimal parameters are compared. All results are given in a normalized form highlighting the influence of the generalized electromechanical coupling coefficient. Comparing the optimal passive LR-network with the optimal LRC-network, it can be shown that damping performance is increased significantly by adding a negative capacitance. An upper limit of the maximum appearing amplitude in the FRFs has been given. For RC- and RLC-networks the maximum amplitudes are, respectively, 3 and 2.38 times the static displacement for the system without negative capacitance. Furthermore, smaller values for resistance and inductance are required. An optimal value for the negative capacitance is given and the stability boundary is derived. It is also shown that the absorbing effect is increased by a negative capacitance resulting in a broader frequency range between the resonances.

These analytical results are verified experimentally. A test rig has been built and a circuit representing the negative capacitance has been implemented. Beside a reduction of the required inductance from 640 to 90 mH, the absorbing effect of an L-network has been increased significantly by adding a negative capacitance, resulting in an absorbing area nearly 3 times larger than before. Also the increased damping performance has been validated, where the maximum appearing amplitude has been reduced to 60% compared to the LR-network.

Acknowledgments

The authors would like to thank Mr. Lindner and Mr. Baldermann. Without their help the experimental results would not have been possible.

References

[1] N.W. Hagood, A.H. von Flotow, Damping of structural vibrations' with piezoelectric materials and passive electrical networks, *Journal of Sound and Vibration* 146 (2) (1991) 243–268.
[2] L.R. Corr, W.W. Clark, Comparison of low-frequency piezoelectric switching shunt techniques for structural damping, *Smart Materials and Structures* 11 (2002) 370–376.
[3] R.A. Morgan, K.W. Wang, An active–passive piezoelectric absorber for structural vibration control under harmonic excitations with time-varying frequency—part 1: algorithm development and analysis, *Journal of Vibration and Acoustics* 124 (2002) 77–83.
[4] D. Niederberger, A. Fleming, S.O.R. Moheimani, M. Morari, Adaptive multi-mode resonant piezoelectric shunt damping. *Smart Materials and Structures* (2004) 1025–1035.
[5] J. Tang, K.W. Wang, Active–passive hybrid piezoelectric networks for vibration control: comparisons and improvement, *Smart Materials and Structures* 10 (2001) 794–806.
[6] M. Date, M. Kutani, S. Sakai, Electrically controlled elasticity utilizing piezoelectric coupling, *Journal of Applied Physics* 87 (2) (2000).
[7] E. Fukada, M. Date, K. Kimura, T. Okubo, H. Kodama, P. Mokry, K. Yamamoto, Sound isolation by piezoelectric polymer films connected to negative capacitance circuits, *IEEE Transactions on Dielectrics and Electrical Insulation* 11 (2) (2004).
[8] J.J. Hollkamp, Multimodal passive vibration suppression with piezoelectric materials and resonant shunts, *Journal of Intelligent Material Systems and Structures* 5 (1994) 49–57.
[9] S. Behrens, S.O.R. Moheimani, A.J. Fleming, Multiple mode current flowing passive piezoelectric shunt controller, *Journal of Sound and Vibration* 266 (2003) 929–942.
[10] S.Y. Wu, Method for multiple mode shunt damping of structural vibration using a single PZT transducer, *Proceedings of the SPIE Smart Structures and Materials*, *Smart Structures and Intelligent Systems*, vol. 3327, Huntington Beach, CA, March 1998, SPIE, pp. 159–68.
[11] A.J. Fleming, S. Behrens, S.O.R. Moheimani, Reducing the inductance requirements of piezoelectric shunt damping systems, *Smart Materials and Structures* 12 (2003) 57–64.
[12] H. Ahlers, Passive Dämpfung reibungsinduzierter Bremsgeräusche mit Piezoelementen, IFW Universität Hannover 2002, ISBN 3-18-335401-2.